arXiv:0802.1071v1 [astro-ph] 7 Feb 2008

The infrared spectra of very large, compact, highly symmetric, polycyclic aromatic hydrocarbons (PAHs)

Charles W. Bauschlicher, Jr.[1], Els Peeters[2,3,4], Louis J. Allamandola[5]

ABSTRACT

The mid-infrared spectra of large PAHs ranging from $C_{54}H_{18}$ to $C_{130}H_{28}$ are determined computationally using Density Functional Theory. Trends in the band positions and intensities as a function of PAH size, charge and geometry are discussed. Regarding the 3.3, 6.3 and 11.2 μm bands similar conclusions hold as with small PAHs.

This does not hold for the other features. The larger PAH cations and anions produce bands at 7.8 μm and, as PAH sizes increases, a band near 8.5 μm becomes prominent and shifts slightly to the red. In addition, the average anion peak falls slightly to the red of the average cation peak. The similarity in behavior of the 7.8 and 8.6 μm bands with the astronomical observations suggests that they arise from large, cationic and anionic PAHs, with the specific peak position and profile reflecting the PAH cation to anion concentration ratio and relative intensities of PAH size. Hence, the broad astronomical 7.7 μm band is produced by a mixture of small and large PAH cations and anions, with small and large PAHs contributing more to the 7.6 and 7.8 μm component respectively.

For the CH out-of-plane vibrations, the duo hydrogens couple with the solo vibrations and produce bands that fall at wavelengths slightly different than their counterparts in smaller PAHs. As a consequence, previously deduced PAH structures are altered in favor of more compact and symmetric forms. In addition, the overlap between the duo and trio bands may reproduce the blue-shaded 12.8 μm profile.

[1]NASA-Ames Research Center, Space Technology Division, Mail Stop 230-3, Moffett Field, CA 94035, USA; Charles.W.Bauschlicher@nasa.gov

[2]Department of Physics and Astronomy, PAB213, University of Western Ontario, London, ON N6A 3K7, Canada; epeeters@uwo.ca

[3]SETI Institute, 515 N. Whisman Road, Mountain View, CA94043, USA

[4]NASA-Ames Research Center, Space Science Division, Mail Stop 245-6, Moffett Field, CA 94035, USA

[5]NASA-Ames Research Center, Space Science Division, Mail Stop 245-6, Moffett Field, CA 94035, USA; Louis.J.Allamandola@nasa.gov

Subject headings: Astrochemistry - Infrared : ISM - ISM : molecules - ISM : molecular data - ISM : line and bands - Line : identification - techniques : spectroscopy

1. Introduction

Polycyclic aromatic hydrocarbons (PAHs) are now thought to be the most plentiful and widespread class of organic compounds in the universe. Their infrared (IR) signature is associated with many different galactic and extragalactic objects (e.g. Cox & Kessler 1999; Helou et al. 2000; Vermeij et al. 2002; Peeters et al. 2004; Bregman & Temi 2005; Brandl et al. 2006; Sellgren et al. 2007; Smith et al. 2007; Galliano et al. 2008), and they account for 10 to 30% of cosmic carbon (Snow & Witt 1995; Puget & Léger 1989; Allamandola et al. 1989; Li & Draine 2001; Draine & Li 2007). For most objects in which the PAH features are present, their spectroscopic signature dominates the mid-IR emission (e.g. Uchida et al. 2000; Verstraete et al. 2001; Peeters et al. 2002b, 2004; Onaka 2004; Sloan et al. 2005; Brandl et al. 2006). It is well established that ionization of PAH molecules dramatically enhances the emission in the 6-9 μm region, suggesting that most of the observed IR emission arises from highly vibrationally excited cations. This excitation generally proceeds via the absorption of ultraviolet (UV), visible (Vis), and near-IR (NIR) radiation (e.g. Li & Draine 2002; Li 2004; Mattioda et al. 2005). While the early, low to moderate resolution spectroscopic observations suggested that the dominant PAH features are invariant, analysis of higher resolution spectra of many objects revealed that the PAH features vary between different classes of object and spatially within extended objects (e.g. Peeters et al. 2002a; van Diedenhoven et al. 2004; Joblin et al. 2000; Bregman & Temi 2005; Sloan et al. 2005; Compiègne et al. 2007), showing that the details in the emission spectrum depend on, and therefore reflect, the specific PAH molecules present and the conditions within the emission zones.

Most previous work on the IR spectroscopic properties of PAHs focused on species containing about 50 or fewer carbon atoms because large PAHs are not readily available for experimental study and computational techniques for such large systems were not practical. While large PAH accessibility remains limited, computational capabilities have increased and the spectra of large PAHs can be determined with good precision. Here we report and discuss the computational IR spectra of several large, compact, and symmetric PAHs, namely $C_{66}H_{20}$, $C_{78}H_{22}$, $C_{110}H_{26}$, $C_{112}H_{26}$ and $C_{130}H_{28}$. When combined with our previous work on the large PAHs $C_{54}H_{18}$ and $C_{96}H_{24}$ (Bauschlicher & Bakes 2000; Bauschlicher 2002), these spectra provide new insight into the effect of PAH size and structure on their IR spectra. The IR spectra of comparably sized, but less compact and less symmetric, PAHs are discussed in

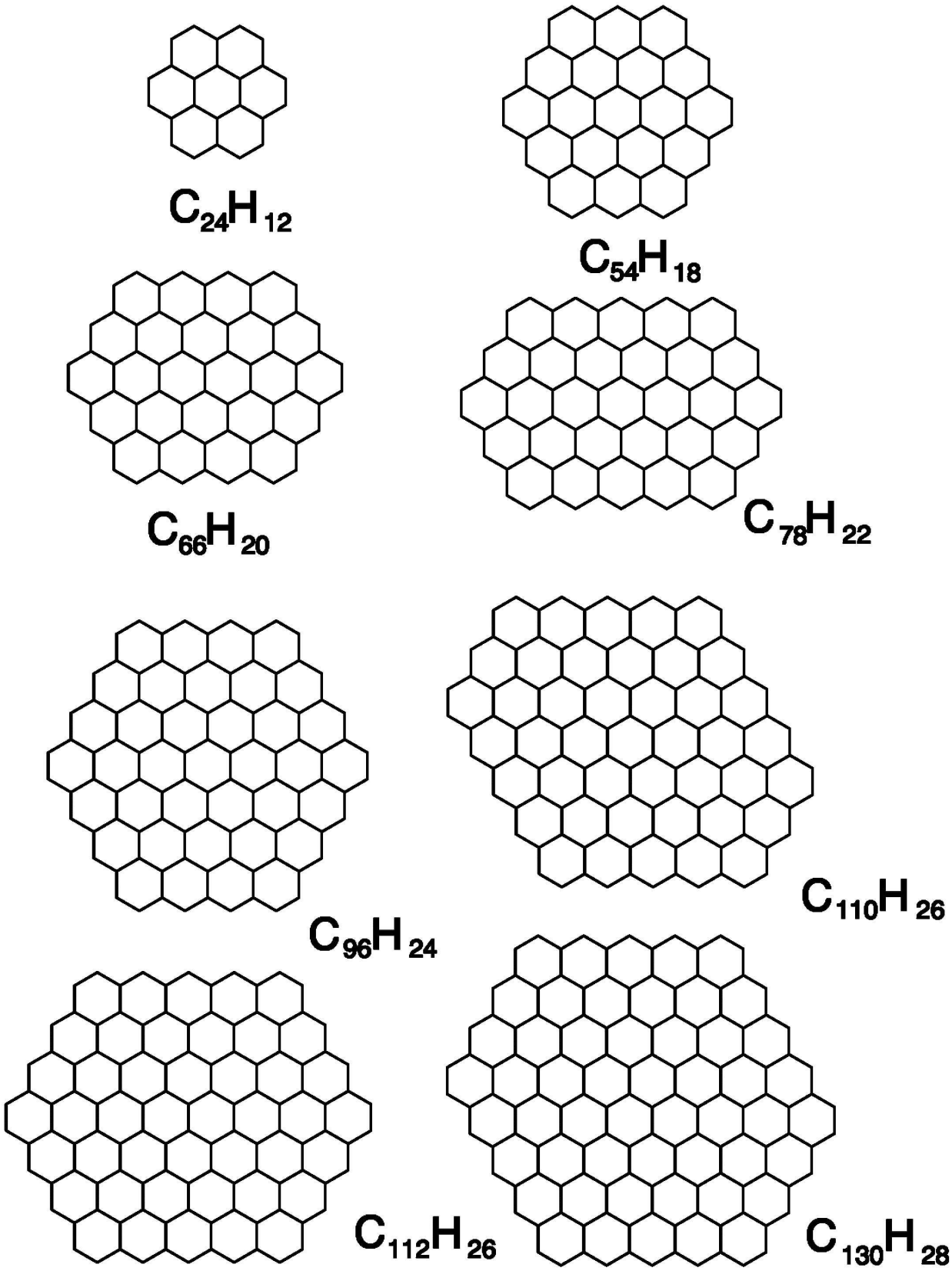

Fig. 1.— The structure of the PAHs studied in this paper.

a subsequent paper (Bauschlicher et al. in preparation, paper II). These two studies, together with the previous work on nitrogen substitution, substantially deepen our understanding of the PAH populations that contribute to the astronomical spectra.

This work is presented as follows. The computational methods used are described in Sect. 2 and the spectra are presented and discussed in Sect. 3. Applications to the astronomical observations and conclusions regarding the astronomical PAH population are given in Sect. 4. The paper is concluded in Sect. 5.

2. Model and Methods

The PAHs considered here are shown in Fig. 1, along with the previously studied coronene ($C_{24}H_{12}$), circumcoronene ($C_{54}H_{18}$), and circumcircumcoronene ($C_{96}H_{24}$) molecules. The spectra for the neutral, cation and anion forms for all these PAHs have been computed. The geometries are optimized and the harmonic frequencies and IR intensities are computed using the B3LYP (Stephens et al. 1994) hybrid (Becke 1993) functional in conjunction with the 4-31G basis sets (Frisch et al. 1984). The calculations are performed using the Gaussian 03 computer codes (Frisch et al. 2003).

The number of bands determined for these large species is so great that we do not show all of the data here. These data are available upon request from the authors and will become part of the publicly available Ames PAH IR Spectral Database which is now under construction. To illustrate these results, synthetic spectra are presented in which the computed frequencies have been scaled by 0.958 and the behavior of some of the more important band positions are discussed. The scaling factor of 0.958 has been found to bring the computationally determined PAH vibrational frequencies into very good agreement with experimentally measured spectra (Langhoff 1996; Bauschlicher & Langhoff 1997). For example, most computational and experimental peak positions fall within 5 cm^{-1} of each other, some within 10 cm^{-1}, and a handful within 15 cm^{-1}. The observed trends in peak position with size and between cations, anions and neutrals should be more accurate than this absolute uncertainty, hence the small shifts we report in this paper should be valid. The intensities are unscaled, despite the potential factor of 2 overestimation of the computed intensity for the CH stretching modes of the neutrals that has been discussed previously (Bauschlicher & Langhoff 1997; Hudgins et al. 2001). To permit comparison of these absorption spectra with astronomical observations which are measured in emission, the natural mid-IR linewidth for a large molecule emitting under interstellar conditions has to be taken into account. Up to now, this has been taken as about 30 cm^{-1} across the mid-IR. As discussed in Cami et al. (in preparation), the natural linewitdth can be band dependent. Here

a linewidth of 30 cm^{-1} is taken for the bands shortward of 9 μm, 10 cm^{-1} for the bands longward of 10 μm, values consistent with current observational and theoretical constraints. For the 9 to 10 μm region, the FWHM is scaled in a linear fashion (in wavenumber space) from 30 to 10 cm^{-1}. In addition to ignoring any further variations of linewidth as a function of mode, Fermi resonances are not taken into account. Despite these limitations, these idealized spectra can be useful in better understanding the astronomical spectra.

3. Results and Discussion

3.1. The C-H stretching vibrations (2.5 - 3.5 μm).

The peak positions of the bands which dominate the CH stretching region for each of the PAHs considered here are listed in Table 1. The spectra are shown in Fig. 2. The peak wavelength for the neutrals is essentially independent of PAH size and falls at ∼3.26 μm. For both the cations and anions however, there is a small shift with increasing size. Including coronene ($C_{24}H_{12}$), the peak wavelength for the cations increases from 3.238 to 3.257 μm with size while that for the anions drops from 3.296 to 3.276 μm with PAH size.

Turning to band strengths, Table 1 shows that the CH stretching (CH_{str}) band intensities increase with PAH size for the neutrals, cations, and anions. While an increase in total band strength with size is to be expected because the number of CH bonds increase with PAH size, the non-additive behavior of the increase is noteworthy. To illustrate this effect, Table 1 also lists the integrated band strengths (A values) per CH for each PAH. Several important points become apparent from this tabulation. First, it is clear that the behavior of coronene is not at all typical for the larger PAHs treated here. This is important because coronene has been considered archtypical of astronomical PAHs, while significantly larger PAHs dominate the cosmic mix. Second, when one removes coronene from further consideration, PAH CH_{str} intensity per CH steadily increases with PAH size for both the cations and neutrals, but much less so for the anions. Third, the CH_{str} intensity drop upon ionization is small for these large PAHs. For example, the integrated intensity per CH for the CH_{str} in neutral $C_{112}H_{26}$ is 41 km/mol and it is 27 km/mol for the cation form. In contrast, consider the A values for coronene in Table 1. Its A value is reduced from 24 km/mol to 5 km/mol, nearly a factor of 5, upon ionization. Significant CH_{str} A value reduction upon ionization is typical for all the small PAHs considered to date (e.g. Langhoff 1996; Bauschlicher & Langhoff 1997; Pathak & Rastogi 2006; Malloci et al. 2007). Thus the dramatic reduction in the A value per CH for the CH_{str} upon ionization that is observed for small PAHs disappears as PAH size increases. This behavior is a consequence of spreading the positive (or negative) charge over more carbon atoms with increasing PAH size, thereby reducing the difference in the CH

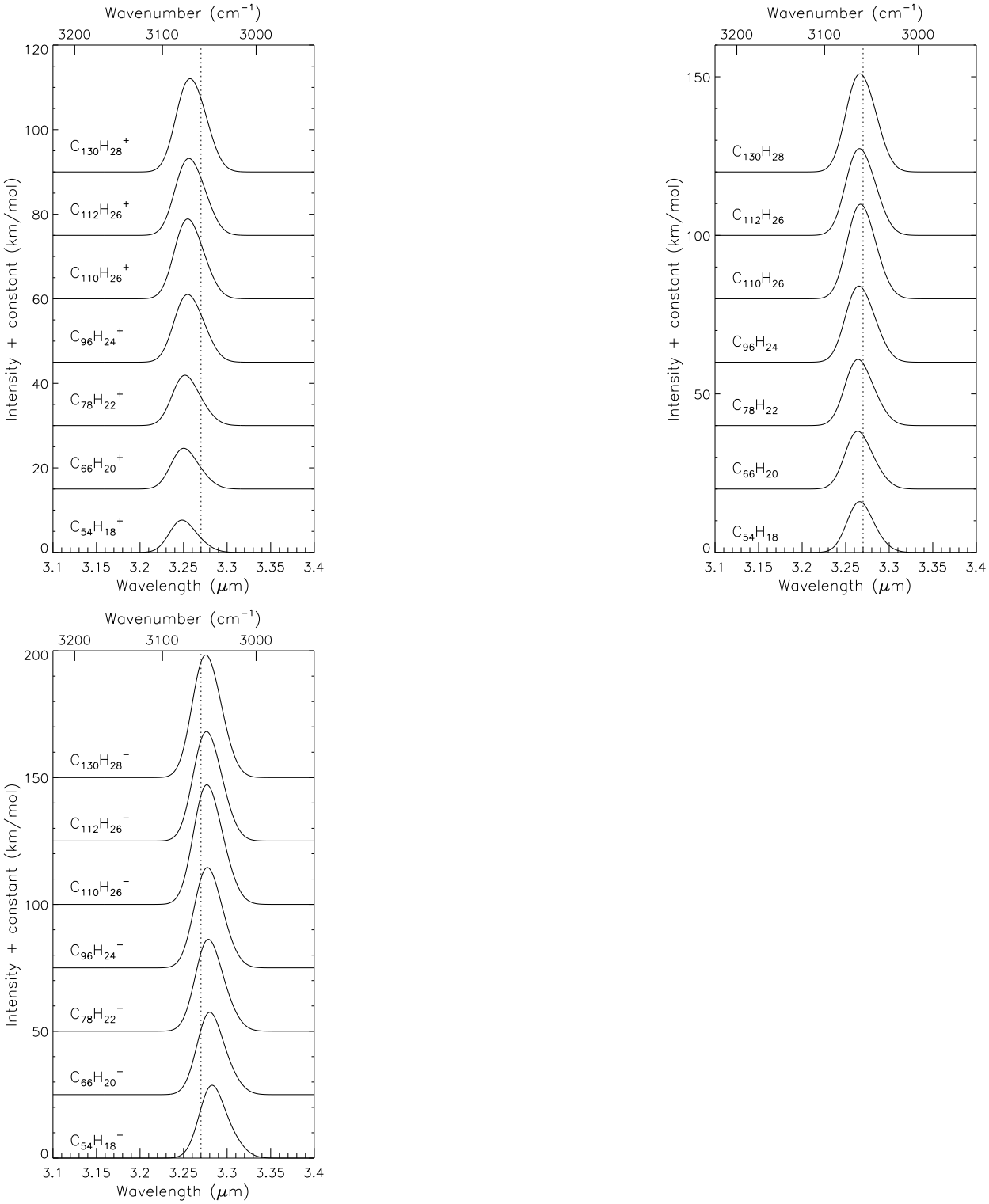

Fig. 2.— The synthetic absorption spectra in the 3 μm region for the large symmetric PAH cations, neutrals and anions considered here. To guide the eye, a dotted line at 3.27 μm is also shown.

stretching dipole derivative between the neutral, cation, and anion, and hence reducing the difference in the observed intensities of the CH stretching vibrations.

3.2. The C-C Stretching and C-H in-plane bending vibrations (5 - 9 μm).

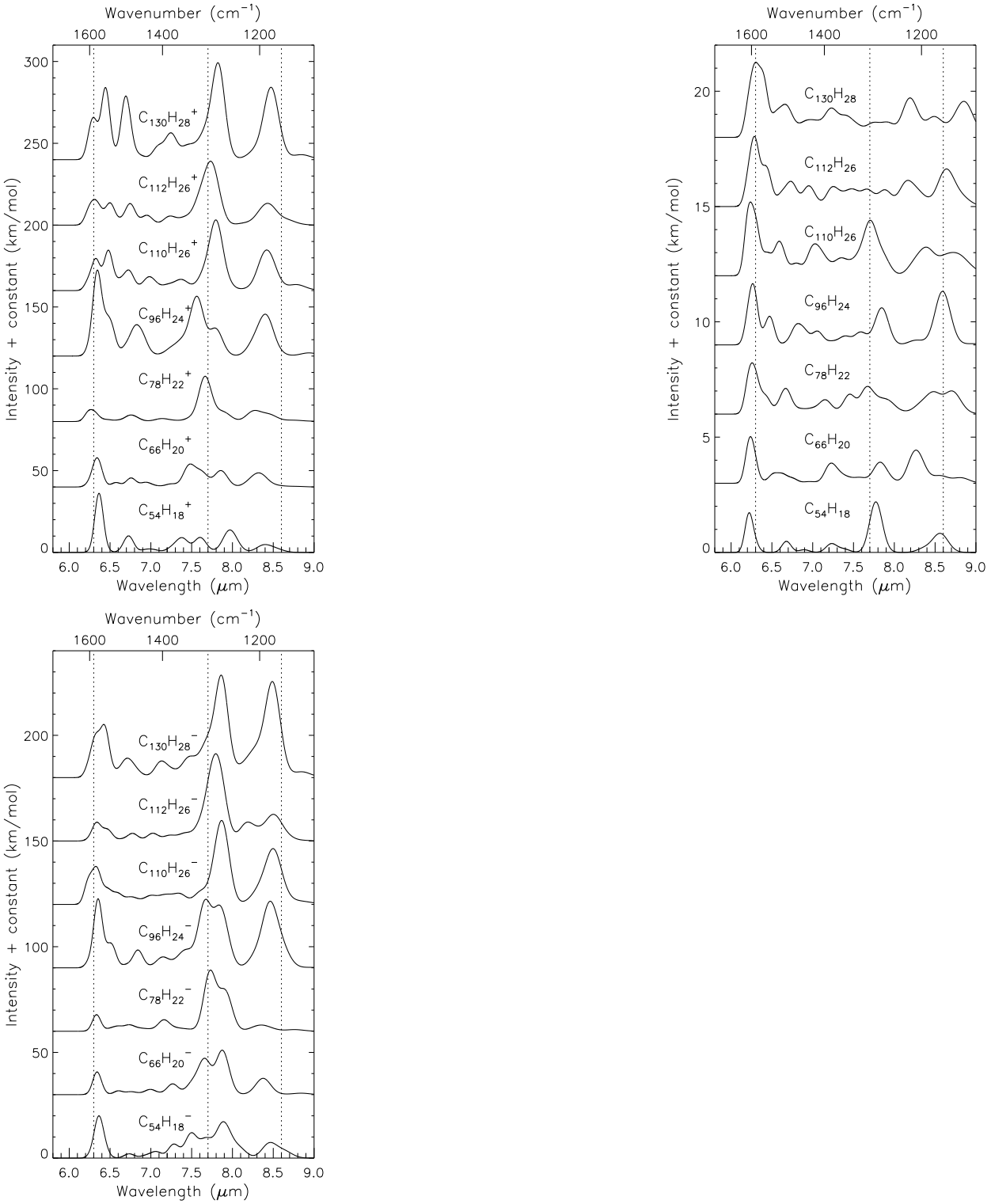

Fig. 3.— The synthetic absorption spectra in the 6 to 9 μm region for the large symmetric PAH cations, neutrals and anions considered here. To guide the eye, dotted lines at 6.3, 7.7 and 8.6 μm are also shown.

Table 1: The C-H stretching band position maximum (λ, in μm), total intensity (I), and intensity per CH (I(CH)) for the PAHs shown in Fig. 1. The intensities are in km/mol.

Molecule	Cation			Neutral			Anion		
	λ	I	I(CH)	λ	I	I(CH)	λ	I	I(CH)
$C_{24}H_{12}$	3.238	58	4.8	3.262	296	24.7	3.296	787	65.6
$C_{54}H_{18}$	3.248	286	15.9	3.266	577	32.1	3.283	1078	59.5
$C_{66}H_{20}$	3.250	365	18.3	3.264	687	34.4	3.280	1208	60.4
$C_{78}H_{22}$	3.252	452	20.6	3.264	800	36.4	3.278	1359	61.8
$C_{96}H_{24}$	3.255	631	26.3	3.265	931	38.8	3.277	1481	61.7
$C_{110}H_{26}$	3.255	731	28.1	3.267	1133	43.6	3.277	1811	69.7
$C_{112}H_{26}$	3.256	716	27.5	3.266	1070	41.2	3.276	1634	62.9
$C_{130}H_{28}$	3.257	871	30.1	3.266	1221	43.6	3.276	1846	65.9

Table 2. The 6-9 μm band position maxima (λ, in μm) and total intensity (I). The intensities are in km/mol.

Molecule	Cation		Neutral		Anion	
	λ	I	λ	I	λ	I
$C_{24}H_{12}$	8.738	53.8	8.771	13.1	8.978	71.6
	8.236	93.2	8.236	2.0	8.216	131.3
			7.620	48.1	7.742	410.1
	7.387	435.3	7.209	1.6	7.374	118.1
					6.825	152.3
	6.650	54.1	6.691	2.7	6.656	23.7
	6.442	465.9	6.240	26.3	6.418	269.2
$C_{54}H_{18}$	8.403	197.2	8.559	31.5	8.467	319.0
	7.969	477.6			7.889	801.4
	7.603	296.4	7.774	70.6	7.686	182.5
					7.501	414.1
	7.378	369.6	7.234	16.5	7.285	202.7
	6.980	86.6	6.894	3.5	7.059	128.1
	6.727	357.4	6.678	15.6	6.735	70.1
	6.365	1189.3	6.223	61.1	6.364	778.2
$C_{66}H_{20}$			8.802	6.9	8.840	23.4
			8.547	8.1		
	8.320	361.9	8.267	52.8	8.376	259.1
	7.857	326.3	7.827	34.4	7.874	695.2
	7.486	756.0	7.567	5.6	7.658	681.5
			7.229	41.9	7.268	174.4
	6.937	97.2	6.962	1.8	6.994	93.5
	6.758	195.7			6.754	45.4
	6.575	77.5	6.557	31.9	6.605	60.7
	6.341	692.7	6.238	77.8	6.341	365.7
$C_{78}H_{22}$			8.701	32.4	8.758	26.1
	8.279	369.3	8.482	39.1	8.354	124.9
	7.665	1181.8	7.672	68.6	7.732	1497.7
			7.457	27.7		

Table 2—Continued

Molecule	Cation		Neutral		Anion	
	λ	I	λ	I	λ	I
	7.140	85.4	7.151	30.7	7.162	261.2
	6.757	190.3	6.669	51.3	6.733	159.8
					6.611	83.7
	6.267	368.5	6.258	123.4	6.335	263.8
$C_{96}H_{24}$	8.938	62.9				
	8.401	1023.3	8.592	77.4	8.463	1352.4
			8.286	4.7		
	7.782	469.8	7.846	56.6	7.833	932.0
	7.563	1816.1	7.590	16.9	7.675	1451.7
			7.404	13.4		
			7.054	20.5	7.151	194.5
	6.827	997.8	6.823	43.8	6.841	313.1
			6.471	41.6	6.497	292.7
	6.345	2718.2	6.265	105.7	6.354	1253.4
$C_{110}H_{26}$	8.776	108.1	8.721	49.5		
	8.420	960.5	8.389	55.4	8.497	1155.5
	7.796	1774.1	7.706	124.1	7.867	1681.3
	7.368	345.2	7.354	27.2	7.335	350.0
	6.983	350.9	7.029	73.1	7.016	157.1
	6.724	500.6	6.799	13.8	6.751	118.1
	6.479	869.9	6.590	62.3		
	6.326	738.8	6.237	175.6	6.326	1293.6
$C_{112}H_{26}$	8.431	644.0	8.639	66.6	8.501	516.5
			8.168	49.2	8.190	297.6
	7.732	1969.1	7.882	22.2	7.795	2046.0
			7.662	23.5		
			7.479	26.4		
	7.241	203.3	7.254	33.8	7.250	73.7
	6.949	197.1	6.952	33.5	7.025	132.6

Table 2—Continued

Molecule	Cation		Neutral		Anion	
	λ	I	λ	I	λ	I
	6.745	492.6	6.730	52.2	6.775	143.7
	6.498	483.8				
	6.308	757.7	6.285	184.7	6.339	503.0
$C_{130}H_{28}$	8.841	90.3	8.852	59.8	8.843	74.6
	8.472	1593.4	8.489	27.9	8.488	1945.1
			8.193	65.4		
	7.822	2666.7	7.899	18.1	7.862	2515.4
			7.768	20.1		
	7.245	835.0	7.231	95.8	7.133	352.2
			6.975	33.4		
	6.694	1392.5	6.660	81.9	6.713	456.8
	6.443	1531.6				
	6.297	811.5	6.303	209.1	6.423	1518.8

The peak wavelengths and integrated band strengths of the important features in the 6-9 μm region of the spectra for the neutral, cation, and anion forms of the PAHs considered here are summarized in Table 2 and the spectra are shown in Fig. 3. The bands in the 6-9 μm region of the spectra correspond to CC stretching and CH in-plane bending vibrations. When considering these results, note that the intensity scale for the spectra of these very large PAHs in the neutral form is at least 10 times smaller than those of the cations and anions. This behavior is consistent with that found for all PAHs studied to date, namely the bands in the 6-9 μm region undergo significant intensity enhancement upon PAH ionization (see Table 2). Since the 6-9 μm bands are rather weak for the neutrals, this discussion will focus on the cations and anions.

Consider first the pure CC stretching region ($\sim$6.2 to 6.5 μm) in the spectra shown in Fig. 3. The spectrum produced by CC stretching vibrations (CC_{str}) of the cations is slightly richer than that of the anions. Nonetheless, the strongest band in this region falls between 6.267 and 6.443 μm in most cases (this excludes $C_{110}H_{26}$ which has two nearly equal peaks at 6.326 and 6.479 μm). The peak position of the CC_{str} features in the spectra of the anions also show less variation than the peak wavelength in the spectra of the cations and they are slightly weaker in both an absolute sense and relative to the bands between 7 and 9 μm. The anion band peak tends to fall at somewhat longer wavelengths than that of the cation, ranging from 6.326 to 6.423 μm. For the three largest PAH cations, there is a second peak in the range 6.443 and at 6.498 μm and a third peak around $\sim$ 6.7 μm. For $C_{130}H_{28}{}^{+}$, the 6.443 μm component is stronger than the 6.297 μm component. There is some surprising variation in the intensity of the cation bands from one molecule to the next, and in this regard note that this band is rather weak for $C_{78}H_{22}{}^{+}$. There are a lot of modes in this spectral range and those with significant intensity derive that intensity from details of the molecular shape and the charge distributed throughout the molecule.

Consider next the bands produced by vibrations involving PAH CC stretching and CH in-plane bending vibrations. These fall from about 7 to 9 μm in the spectra shown in Fig. 3. The features in the 7 to 8 μm region are associated with vibrations in which CC stretching and CH in-plane bending motions are coupled, while those between 8 and 9 μm primarily arise from CH in-plane bending vibrations. The 7 to 9 μm spectra of the cations and anions resemble one another and, at first glance, the spectra of the three largest PAHs appear similar. However, upon closer inspection important differences become evident. The following trends emerge when comparing the spectra.

For the three largest PAHs, the strongest feature near 7.7 μm (the position of the strongest astronomcial feature) falls between 7.732 and 7.822 μm for the cations and between 7.795 and 7.867 μm for the anions. This tendency for the cation bands to fall at slightly

shorter wavelengths than for the anions holds for the smaller PAHs considered here as well, although the spread is somewhat larger.

The variation in peak position of the strongest band near 7.7 μm is less pronounced for the anions than for the cations, mostly because the bands in the small anions tend to fall at longer wavelengths than those in small cations. For example, for $C_{78}H_{22}{}^{+}$ the band falls close to 7.67 μm , but for $C_{96}H_{24}{}^{+}$ the maximum is closer to 7.56 μm. For the corresponding anions, the difference is less than 0.05 μm. The 7.7 μm band of the two smallest PAH cations, $C_{54}H_{18}{}^{+}$, and $C_{66}H_{20}{}^{+}$ is not very pronounced. However, further increasing the size leads to a shift toward $\sim$7.8 μm for the three largest PAH cations considered here.

We turn now to the bands that arise primarily from CH in-plane bending vibrations, the features in the 8 to 9 μm region of the spectra in Fig. 3. Overall, the spectral features of both the anions and cations in this region are rather similar. While there is slight variation in the position of these bands, there appears a general shift to longer wavelength with increasing size of the PAH cation. There is a band in the 8.279 to 8.467 μm range for the three smallest PAHs, but it is not very strong. However, as PAH size increases, the intensity of this band increases significantly and it shifts to longer wavelength, producing the very prominent band that appears near 8.5 μm in the spectra of the 4 largest PAHs for both the cations and anions.

For the molecules studied in this work, there are many allowed modes throughout the spectra. It is therefore interesting to note that for some molecules, a few bands carry all the intensity in the 6-9 μm region, while for others there are several bands with significant intensity. This is very different from the C-H stretching region where the band position varies little for the molecules studied here. Thus, the 6-9 μm region of the spectra may yield some insight into the character of the molecules present in the astrophysical environment. With this in mind, we have viewed the modes that compose the bands that carry significant intensity, for both the molecules in this work and the lower symmetry species presented in paper II. While at the present time we are unable to make a definitive prediction of the nature of the spectra in the 6-9 μm region based on molecular shape, a study of the modes suggests that the differences in the spectra are related to the shape of the edge. We continue to investigate this and will revisit this in paper II.

3.3. The CH Out-of-Plane Bending Vibrations (9 to 15 μm).

Table 3. The 9-15 μm band position maxima (λ, in μm) and total intensity (I, in km/mol). For PAHs with *any* band stronger than 10km/mol, all charge states are listed. If the bands for the cation, neutral and anion state of a PAH all fall below 10km/mol they are not included.

Molecule	Cation		Neutral		Anion	
	λ	I	λ	I	λ	I
$C_{24}H_{12}$	13.098	13.7	12.910	11.7	13.158	16.5
	12.757	32.7			12.835	17.5
	12.422	7.0			12.323	164.8
	11.355	190.5	11.575	175.6	10.752	2.2
$C_{54}H_{18}$	13.922	21.9	13.864	21.7	13.922	17.7
	12.668	53.9	12.788	43.3	13.144	23.3
	11.939	13.2	11.916	10.2	11.710	107.9
	10.881	218.1	11.061	221.1	11.353	128.9
	10.162	46.6	10.167	2.8	10.195	1.4
	9.768	1.3	9.790	12.6	9.835	8.1
	9.186	11.3				
$C_{66}H_{20}$	12.868	1.7	12.702	52.7	12.893	35.1
	12.596	57.4			12.466	1.3
	12.136	10.9	12.270	2.6	12.148	3.4
	11.307	17.4	11.682	7.5	11.567	35.0
	10.984	48.1	11.150	39.1	11.355	232.7
	10.823	194.7	10.995	216.3	10.989	6.0
$C_{78}H_{22}$	14.102	13.5	14.112	10.4	14.178	7.5
	12.653	53.1	12.780	44.4	12.974	27.7
	11.955	5.4	11.942	18.5	11.969	6.8
	11.722	21.9	11.570	4.7	11.783	1.8
	10.971	76.5	11.132	70.5	11.302	301.4
	10.810	198.5	10.966	212.2	10.728	8.0
	10.206	13.6	10.241	5.7	10.262	6.9
	9.347	9.0	9.387	2.0	9.387	16.0
$C_{96}H_{24}$	14.648	9.5	14.639	5.7	14.786	13.8
	13.203	8.6	13.158	6.0	13.293	10.3
	12.677	17.4				
	12.385	76.9	12.477	74.2	12.606	65.8

Table 3—Continued

Molecule	Cation		Neutral		Anion	
	λ	I	λ	I	λ	I
					11.338	162.7
	10.825	299.0	10.959	316.4	11.120	199.6
	9.630	29.7	9.630	21.4		
	9.334	49.3	9.341	3.2	9.369	18.9
$C_{110}H_{26}$	14.535	16.2	14.539	13.1	14.560	11.5
	13.040	9.3	13.098	6.2	12.933	70.5
	12.655	55.4	12.749	46.1	12.557	6.8
	12.090	4.2	12.070	4.3	12.053	51.6
	11.686	28.0	11.820	25.6	11.741	3.7
	11.400	8.0	11.370	7.8	11.549	20.1
	11.183	14.7			11.177	350.4
	11.023	26.1				
	10.814	316.7	10.954	348.6	10.875	3.7
	10.134	11.0	10.128	4.8	10.148	3.1
	9.458	45.4	9.349	22.4	9.461	49.8
$C_{112}H_{26}$	12.466	67.0	12.544	54.1	12.692	53.3
	12.099	7.3	12.109	4.4	12.226	17.8
	11.716	15.2	11.846	12.9	11.640	22.3
	10.820	324.3	10.941	341.2	11.148	356.1
	10.122	15.7	10.139	4.8	10.301	16.1
	9.620	16.1	9.620	17.5	9.547	20.9
	9.291	38.8	9.297	8.1	9.322	14.1
$C_{130}H_{28}$	14.019	9.1	14.071	7.4	14.233	29.3
	12.587	66.5	12.703	59.6	12.706	69.5
					12.047	16.4
					11.902	44.4
	11.660	36.1	11.802	29.1	11.610	25.9
	11.085	10.2	11.498	9.0	11.116	383.5
	10.817	351.2	10.936	369.8		
	10.138	21.9	10.167	8.8	10.166	54.1

Table 3—Continued

Molecule	Cation		Neutral		Anion	
	λ	I	λ	I	λ	I
	9.836	26.0			9.853	7.6
	9.575	23.7	9.574	12.3	9.602	5.0

Table 4: The total intensity (I, in km/mol) and intensity per CH (I(CH), in km/mol) for the solo and duo modes.

Molecule	Mode	Cation		Neutral		Anion	
		I	I(CH)	I	I(CH)	I	I(CH)
coronene	solo	220.67	36.78	221.08	36.85	128.89	21.48
	duo1	14.89	1.24	10.28	0.86	114.67	9.56
	duo2	53.86	4.49	43.33	3.61	23.33	1.94
$C_{66}H_{20}$	solo	260.12	32.51	255.46	31.93	238.30	29.79
	duo1	69.11	5.76	10.08	0.84	40.22	3.35
	duo2	1.74	0.14	52.71	4.39	35.05	2.92
$C_{78}H_{22}$	solo	275.02	27.50	282.71	28.27	301.39	30.14
	duo1	34.34	2.86	25.41	2.12	12.20	1.02
	duo2	59.44	4.95	50.50	4.21	30.84	2.57
$C_{96}H_{24}$	solo	299.05	24.92	316.42	26.37	362.34	30.20
	duo1	82.03	6.84	76.98	6.42	1.56	0.13
	duo2	17.53	1.46	6.01	0.50	65.78	5.48
$C_{110}H_{26}$	solo	365.42	26.10	356.38	25.46	354.08	25.29
	duo1	32.27	2.69	29.85	2.49	82.29	6.86
	duo2	64.72	5.39	52.29	4.36	70.56	5.88
$C_{112}H_{26}$	solo	325.01	23.22	341.21	24.37	356.13	25.44
	duo1	89.47	7.46	79.95	6.66	40.12	3.34
	duo2	7.85	0.65	15.81	1.32	61.65	5.14
$C_{130}H_{28}$	solo	361.41	22.59	369.77	23.11	383.45	23.97
	duo1	102.59	8.55	38.10	3.17	86.72	7.23
	duo2	6.36	0.53	66.25	5.52	77.49	6.46

The 9 to 15 μm region of the spectra for the neutral, cation, and anion forms of the PAHs considered here are shown in Fig. 4 and the peak wavelengths and integrated band strengths of the most significant bands in these spectra are summarized in Table 3. The bands shown in Fig. 4 correspond to CH out-of-plane bending vibrations (CH_{oop}). In contrast with the spectra in the 5 to 9 μm region, the intensities of the CH_{oop} bands for all three PAH charge forms are very similar. In all three cases, the larger the PAH the shorter the wavelength of the strongest feature.

Perusal of Fig. 1 shows that there are only solo and duo hydrogens on the PAHs considered here. For these PAHs, the CH_{oop} band for the solo hydrogens falls between 10.936 and 11.061 μm for the neutral forms, between 10.810 and 10.881 μm for the cations, and between 11.116 and 11.353 μm for the anions (see Fig. 4). These all fall within the broader range for solo hydrogens on smaller PAHs (Hudgins & Allamandola 1999, and references therein). However, this generalization doesn't hold for the bands produced by duo hydrogen vibrations on these larger PAHs. Analysis of the vibrations of these larger PAHs shows that the CH_{oop} vibrations for duo hydrogens produces two bands: a weaker one between $\sim$11.5 and 12 μm and a stronger one near $\sim$12.8 μm. The weaker band lies in the region normally associated with duo CH_{oop} vibrations while the more prominent band falls in the region normally attributed to trio adjacent hydrogens, yet none of these PAHs have trio hydrogens. Furthermore, the weak duo band peaking near 11.5-12 μm shows less variation in peak position than does the duo band near $\sim$12.8 μm. The strongest of the bands produced by duo CH_{oop} bends for the neutral and cation species considered here fall just below 12.8 μm while half of the PAH anion duo band peaks lie above 12.8 μm and half below. Interestingly, the spectrum of coronene ($C_{24}H_{12}$), a small PAH with only duo hydrogens, shows a prominent band at 11.575 μm as well as a weak band at 12.910 μm (see Table 3 Hudgins & Allamandola 1999).

The intensities of these bands are listed in Table 4. Inspection of this Table 4 reveals trends in the A-values per CH for the bands produced by the CH_{oop} vibrations that differ significantly from those in small PAHs. Excluding the entries for coronene, the average A value per CH for the solo hydrogens[1] in the cation, neutral, and anion charge states of the very large PAHs are 26 km/mol, 27 km/mol, and 27 km/mol respectively. These values are about twice the average A values for the neutral (13 km/mol) and cation forms (14 km/mol) of smaller PAHs Hony et al. (2001). Similarly, the average for the duo modes[2] of the very large PAHs considered here are 7.7 km/mol, 7.0 km/mol, and 7.2 km/mol for the cation,

[1] 10.8-11.4 μm range

[2] 11.4-12.6 and 12.6-13.2 μm ranges

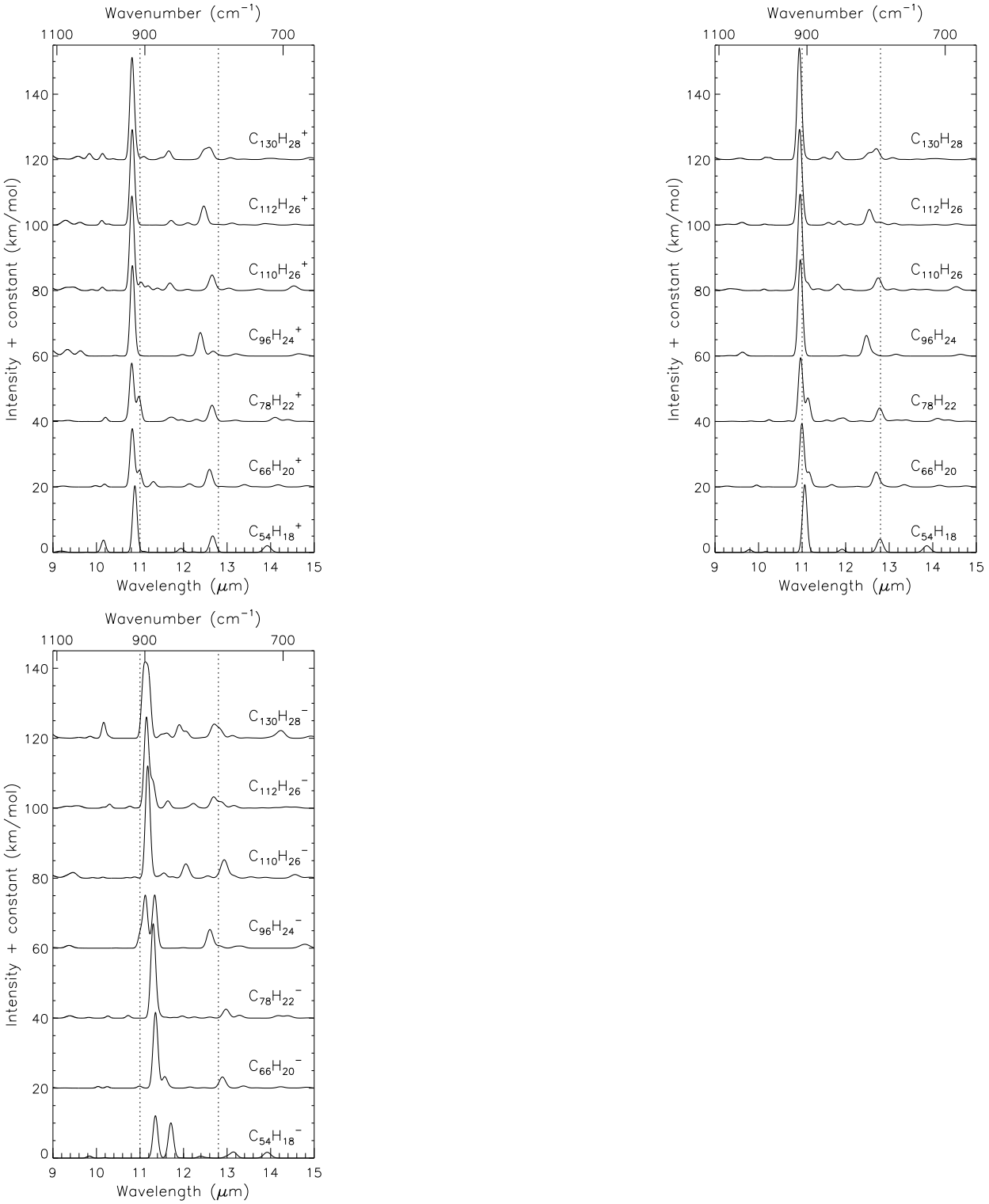

Fig. 4.— The synthetic absorption spectra in the 9 to 15 μm region for the large symmetric PAH cations, neutrals and anions considered here. To guide the eye, dotted lines at 11.0 and 12.8 μm are also shown.

neutral and anion forms versus 2.5 km/mol and 2.4 km/mol for the cation and neutral forms of the smaller PAHs. The ratio of solo-to-duo hydrogens in the PAHs considered here spans the range from 1.3 ($C_{130}H_{28}$) to 0.5 ($C_{54}H_{18}$). The relative intensities of the corresponding bands in Figure 4 reflects the constancy of the A-values; independent of the PAHs in this sample. It is important to note that the A-values for the duo modes in the smaller PAHs were determined from PAHs with structures that included solo, trio, and quadrupule hydrogens. The larger, symmetric, compact PAHs discussed here are quite different in this respect. As they are of a size comparable to those that dominate the astronomical PAH mix, the conclusions derived here and in paper II are more appropriate for the emitting astronomical PAH population.

To gain more insight into the origin of the variation of the duo hydrogen modes, the force constants for neutral $C_{110}H_{26}$ were used to recompute the vibrational spectra, but with the mass of either the solo or duo hydrogens changed from 1.00783 (hydrogen) to 0.2 AMU. While a mass of 0.2 AMU is completely artificial, this change in mass shifts the CH_{oop} modes of the altered mass hydrogens out of the 9-15 μm region and eliminates the vibrational coupling between the solo and duo hydrogens. The result of this numerical experiment is shown in Fig. 5. Note that the FWHM is reduced to 7 cm^{-1} in these spectra to more clearly show the changes. Comparing the spectrum of $C_{110}H_{26}$ with that in which the mass of the duo hydrogens is reduced shows that the coupling with the duo hydrogens increases the intensity of the solo peak at 11 μm and shifts it very slightly in wavelength. The small solo peak near 11.2 μm is reduced in intensity and shifted slightly to shorter wavelength when coupled to the duo hydrogens. The duo bands without coupling are reasonably strong and fall near 12.3 μm, but when coupled to the solo band, they lose intensity and are split into two bands, one near 11.8 μm and the other at 12.8 μm. The duo bands show a much more dramatic change with coupling than the solo bands for these large compact PAHs which have comparable amounts of solo and duo hydrogens.

4. Astrophysical Implications

The mid-IR spectroscopic properties of the large PAHs presented above will now be compared with observations. The discussion parallels the order in Sect. 3.

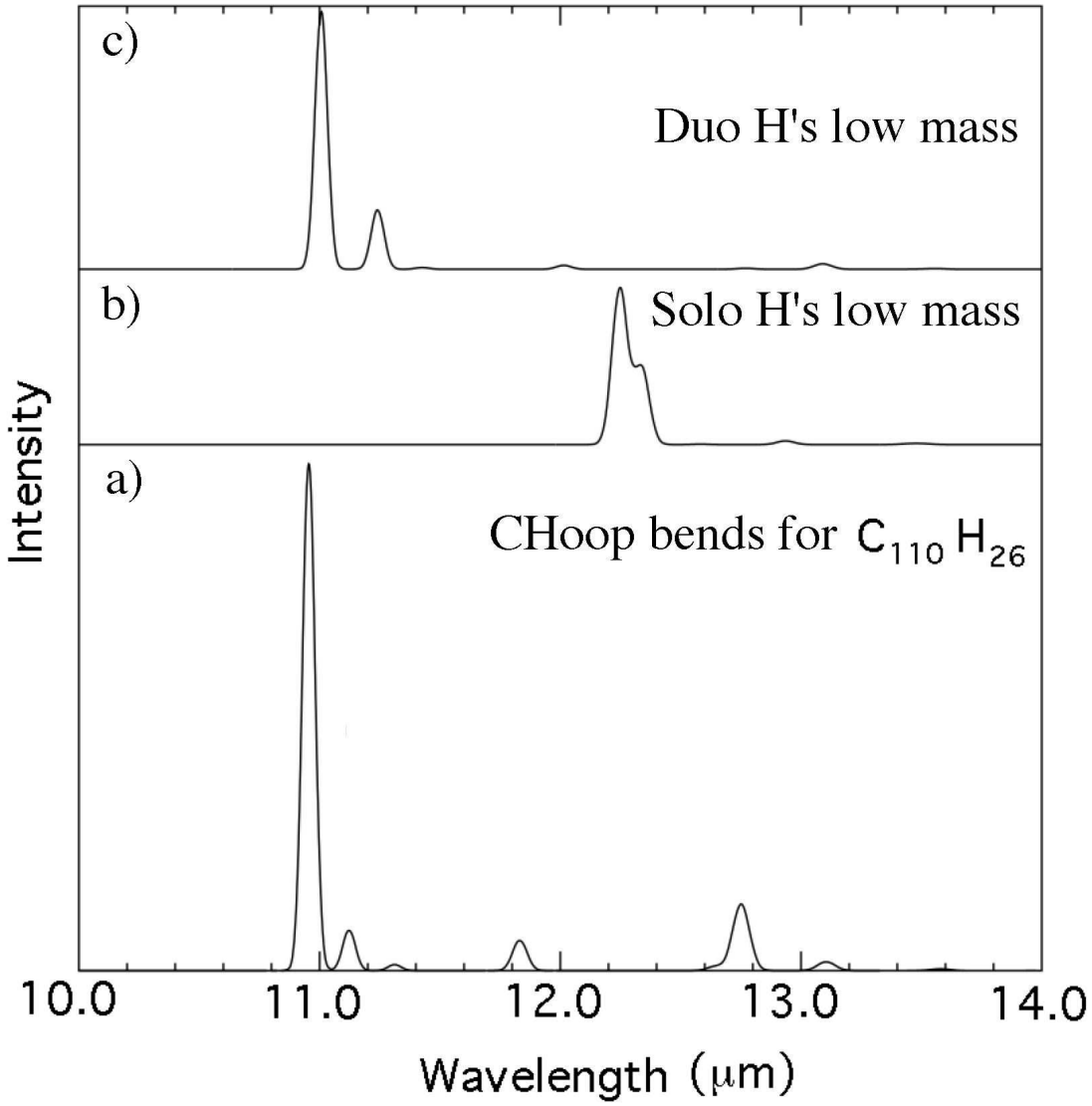

Fig. 5.— The influence of hydrogen mass on the CH_{oop} bands of $C_{110}H_{28}$. a) The spectrum of normal $C_{110}H_{28}$; b) The computed spectrum with the mass of the solo hydrognes artificially reduced to 0.2 AMU; c) The computed spectrum with the mass of the duo hydrogens artificially reduced to 0.2 AMU.

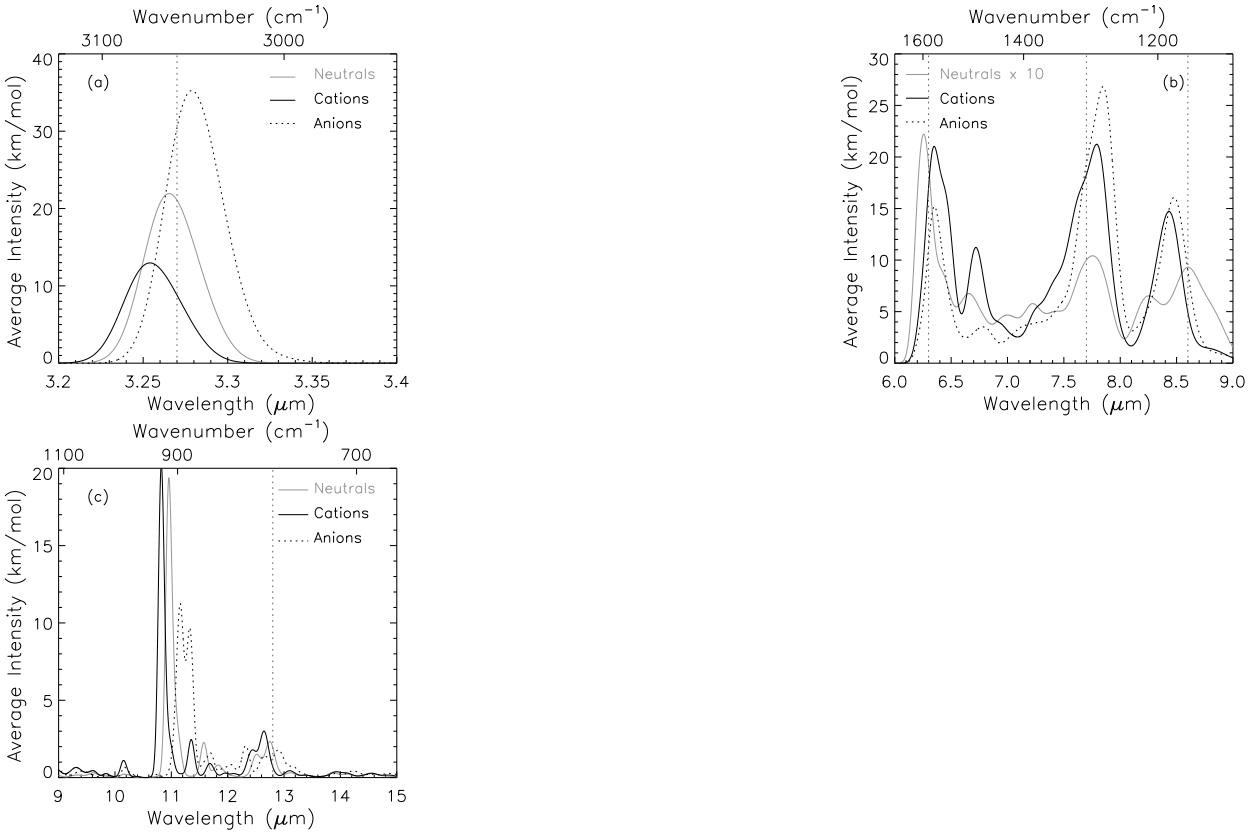

Fig. 6.— The average of the synthetic absorption spectra for the large symmetric PAH cations, neutrals and anions considered here. To guide the eye, dotted lines at 3.27, 6.3, 7.7, 8.6 and 12.8 μm are also shown.

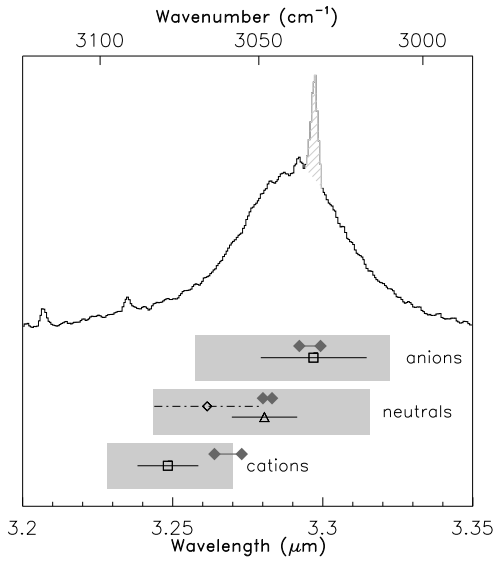

Fig. 7.— Comparison of the astronomical emission feature from NGC 7027 (class $A_{3.3}$) with the peak positions of the CH stretch in various PAHs. The striped, narrow grey feature in the spectrum of NGC7027 is the Pfδ line. The PAH data are redshifted by 15 cm^{-1}, a shift which is intrinsic to the emission process (see text for details). The connected, filled diamonds indicate the range of the CH stretch in the large PAHs considered here. The shaded horizontal bars indicate the full range of the PAH CH stretching modes for the smaller PAH sample described in the text (Sect. 4.1). The symbols crossed by short horizontal lines represent the average wavelength and standard deviation for that bar. The open diamond and triangle in the bar for neutral PAHs show the average and standard deviations for peak positions of PAHs containing ≥ 40 and < 40 C atoms, respectively, in the previous data set. Figure adapted from van Diedenhoven et al. (2004).

.

4.1. The C-H stretching vibrations (2.5 - 3.5 μm).

The astronomical emission bands arising from the CH stretching vibrations were discussed in detail by van Diedenhoven et al. (2004). These authors compared their astronomical data with experimental and theoretical spectra of over 100 small PAHs ($< C_{40}$) in their neutral and positively charged states, supplemented by the spectra of a few larger PAHs, and 27 small PAH anions. This analysis is extended here to include the impact of the spectrum of the larger PAHs shown in Fig. 1 on the earlier conclusions.

Fig. 6a shows the feature produced by averaging the bands associated with each charge state previously presented in Fig. 2. This clearly demonstrates the shift in peak position as a function of PAH charge. Fig. 7 shows the 3.29 μm astronomical emission feature from NGC 7027 along with grey bars which represent the full range of PAH CH stretching peak positions for the neutral, cationic, and anionic PAHs in the sample described above. Superposed on this figure is the range in peak positions for the very large compact PAHs presented in Table 1 (dark grey bar connecting filled diamonds). To facilitate the comparison between the spectra presented here and the astronomical spectra, all laboratory and theoretical spectra have been redshifted by 15 cm^{-1} to take the redshift into account that is intrinsic to the emission process (Flickinger et al. 1991; Brenner & Barker 1992; Colangeli et al. 1992; Joblin et al. 1995; Williams & Leone 1995; Cook & Saykally 1998). The peak positions for compact, very large PAHs fall within the regions spanned by the earlier sample, but span a much narrower range. Consequently, the principle conclusion presented in van Diedenhoven et al. (2004) for this feature, namely that its peak position is most consistent with an origin in neutral and negatively charged PAHs, while clearly ruling out an origin in PAH cations, remains unaltered. The proximity of the ranges in the CH_{str} peak position for the neutral and anion PAH forms suggests that the two classes of astronomical 3.3 μm band designated as $A_{3.3}$ and $B_{3.3}$ by van Diedenhoven et al. (2004) reflect the relative contributions of PAH neutrals and anions.

The narrow range in CH stretch frequencies listed in Table 1 and illustrated in Fig. 7, and the predominance of one feature in the CH stretching region are characteristics inherent in the spectroscopy of compact and largely symmetric PAHs. Such structures require that the molecules have similar edge structures. This, in turn, leads to similar spectra involving the CH modes as the local environment of each peripheral CH group is similar along the edge of the molecule within a given molecule and from one molecule to the next. The similarity between the absorption band of the CH stretch in the large compact PAHs described here and the astronomical 3.29 μm feature suggests that compact and somewhat symmetric PAH cations and anions dominate the PAH mixture producing this astronomical feature. This aspect of very large PAH spectroscopy will be further discussed in paper II.

4.2. The C-C Stretching and C-H in-plane bending vibrations (5 - 9 μm).

The 5 to 9 μm astronomical emission bands arising from PAH CC stretching and CH in-plane bending vibrations were discussed in great detail by Peeters et al. (2002a). Their analysis was based on a dataset of experimental and theoretical spectra similar to that described in Sect. 4.1 above and is extended here to include the spectroscopy of the larger PAHs shown in Fig. 1. Fig. 6b shows the average 6 - 9 μm spectra of these PAHs in their neutral, cation, and anion forms. The corresponding spectra of the neutral PAHs will not be considered further here as their absorption band intensities are at least an order of magnitude smaller than those of the corresponding cations and anions.

Consider first the spectroscopy near 6.2 to 6.3 μm, the region attributed to pure CC stretching vibrations. Summarizing Sect. 3.2, the CC_{str} features in the spectra of the anions show less variation than the spectra of the cations and they are slightly weaker in both an absolute sense and relative to the bands between 7 and 9 μm. Nonetheless, Figure 6b shows that the average spectrum of the cations and anions is dominated by a band that peaks near 6.3 μm, close to the well-known astronomical emission band that peaks between 6.2 and 6.3 μm, depending on the object type (Peeters et al. 2002a). The spectra presented here extend our earlier finding, that the pure CC stretch in PAHs comprised of only C and H cannot reproduce the observed peak position of corresponding astronomical feature, to very large PAHs (note that the redshift of 15 cm^{-1} is not applied to Figure 6 and hence in emission, the bands will fall longwards of the astronomical class A 6.2 PAH band). This supports our previous conclusion that pure PAH molecules cannot reproduce the 6.2 μm component (Class A in Peeters et al. 2002a) of the astronomical emission feature, leading to the suggestion that astronomical PAHs contain nitrogen (PANHs, Peeters et al. 2002a; Hudgins et al. 2005). In this regard, it is important to recall that the 6 - 9 μm bands in neutral PANHs have absorption strengths half as large as do PAH ions.

It is interesting to note that the cations and anions of several of these large symmetric species have bands in the 6.7-6.8 μm region, in particular for $C_{96}H_{24}$ and $C_{130}H_{28}$. Bands in this region are often thought to arise from CH deformations in aliphatic side-groups. To better understand the origin of the bands in the region, more calculations on large PAHs are required.

Turning to the features near 7.7 μm, Fig. 3 shows that the cations and anions of the PAHs considered here have strong bands close to this position. For the cations, as the PAH size increases this band tends to shift to longer wavelength but there is some variation in position with PAH. For the anions, the band seems to fall closer to 7.8 μm and is less dependent on the size of the PAH. The average spectra in Figure 6b show that the strong feature produced by both the cations and anions overlap to a large extent, but that the

average anion peaks about 0.1 μm to the red of the average cation peak. Together, these and earlier data suggest that the astronomical 7.7 μm band is produced by a mixture of small and large PAH cations and anions, with small PAHs contributing more to the 7.6 μm component and large PAHs more to the 7.8 μm component. Peeters et al. (2002a) showed that when the 7.8 μm component dominates the 7.7 μm complex, its peak position varies between 7.8 and 8 μm. Given the slight difference in peak position between large PAH cations and anions, this suggests that negatively charged PAHs contribute more to the red portion of the 7.8 μm component than do PAH cations.

Lastly, for both anions and cations, a band near 8.5 μm grows in strength as PAH size increases (Figure 3). Figure 6b shows that the bands from both the large PAH anions and cations overlap, again with the anions contributing more strongly at slightly longer wavelengths. Peeters et al. (2002a) found a correlation between the peak of the astronomical 7.8 μm component of the 7.7 μm feature, and the peak position of the 8.6 μm band, i.e. they both are redshifted by a similar relative degree. The failure of small PAHs to reproduce i) the 7.8 μm emission component, ii) a prominent 8.6 μm emission feature and iii) the correlation between the peak position of the astronomical 7.7 μm feature and the 8.6 μm band suggest that both the 7.8 μm component and the 8.6 μm band originate primarily in large, cationic and anionic PAHs, with the specific peak position and profile reflecting the particular cation to anion concentration ratio in any given object.

Fig. 8 compares the emission spectrum from the HII region IRAS 23133+6050 and the Red Rectangle to the average spectrum produced by the large PAHs computed here and an earlier "best fit", average mixture of smaller PAHs [3]. The following constraints and conclusions regarding the emitting astronomical PAH population can be drawn from this comparison. First, the overall agreement between the astronomical emission spectrum and the simple average PAH spectrum lend general support to the PAH model. Second, the peak of the dominant band in the CC stretching region for both small and large pure PAHs falls longwards of the observed 6.2 μm position, reiterating the need to alter this fundamental vibration in some way. The substitution of nitrogen for some of the carbon atoms satisfies this constraint. Third, the spectra shown here suggest that the overall profile of the 7.7 μm feature, with components at 7.6 and 7.8 μm, may be accommodated by emission from a PAH population that includes large and small PAHs. The discussion above

[3]The composite spectrum of 11 PAHs consists out of 22% neutral coronene ($C_{24}H_{12}$); 19% 3,4;5,6;10,11;12,13-tetrabenzoperopyrene cation ($C_{36}H_{16}^{+}$); 15% coronene cation ($C_{24}H_{12}^{+}$); 7% dicoronylene cation ($C_{48}H_{20}^{+}$); 7% benzo[b]fluoranthene cation ($C_{20}H_{12}^{+}$); 7% benzo[k]fl uoranthene cation ($C_{20}H_{12}^{+}$); 7% neutral naphthalene ($C_{10}H_{8}$); 4% naphthalene cation ($C_{10}H_{8}^{+}$); 4% phenanthrene cation ($C_{14}H_{10}^{+}$); 4% chrysene cation ($C_{18}H_{12}^{+}$); 4% tetracene cation ($C_{18}H_{12}^{+}$).

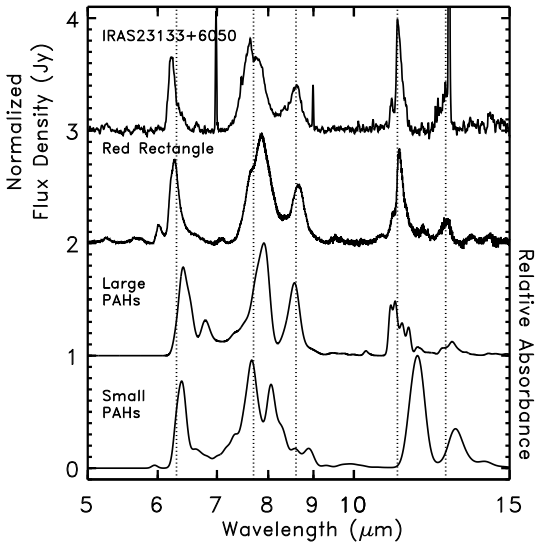

Fig. 8.— Astronomical PAH emission spectra from 5 to 15 μm compared with the spectra of PAH mixtures. Shown are the continuum subtracted ISO-SWS spectrum of IRAS23133+6050 representing class A PAH profiles **(top)**; the continuum subtracted ISO-SWS spectrum of the Red Rectangle, representing class B PAH profiles **(second)**; the average spectrum of the large symmetric PAH cations, neutrals and anions considered here **(third)**; and the composite absorption spectrum generated by co-adding the individual spectra of 11 PAHs, reproduced from Peeters et al. (2002a, see text for composition) **(bottom)**. A redshift of 15 cm^{-1}, intrinsic to the emission process, has been applied to the positions of the large and small PAH spectra. To guide the eye, dotted vertical lines are also shown.

also suggests that, in addition to larger PAHs contributing strongly to the 7.8 μm component (dominant in Class B profiles), PAH anions contribute more to the longer wavelengths than do PAH cations, consistent with the spatial variation of the 7.8 μm component in NGC 2023 (Bregman & Temi 2005). Fourth, a prominent peak near 8.6 μm appears only in the spectra of larger PAHs, suggesting that the relative intensity of the 8.6 μm astronomical band to the other astronomical bands can be taken as an indicator of the relative amounts of large to small PAHs in the emitting population. For example, the 8.6 μm feature is barely evident on the wing of a strong 7.7 μm feature in some objects (e.g. IRAS07027-7934, IRAS21190+5140), while it is prominent in others such as the objects shown here, and it can be as intense at the 7.7 μm band itself in others (e.g. MWC 922). In addition, large PAH anions are most likely responsible for the red-shifted 8.6 μm feature.

4.3. The CH Out-of-Plane Bending Vibrations (9 to 15 μm).

The astronomical emission bands arising from the CH_{oop} bending vibrations were discussed in detail by Hony et al. (2001). Their analysis was based on a detailed experimental study of 20 PAHs which sampled the different edge structures possible and which range in size from $C_{10}H_8$ to $C_{32}H_{14}$ (Hudgins & Allamandola 1999). Here we extend this analysis to larger PAHs and assess the earlier conclusions.

The PAH bands in the CH_{oop} region are used to gain insight into the relative number of solo, duo, trio, and quartet hydrogens on astronomical PAHs and perhaps provide some insight into their charge distribution. Indeed, the relative intensities of these bands have been used to determine the relative amounts of the different types of peripheral CH groups present in the emitting astronomical PAH population and constrain astronomical PAH molecular structures. In addition, comparing the relative intensities of the CH_{oop} bands with the PAH emission features at shorter wavelengths and searching for interband correlations has been used to further constrain structures. This analysis has led to the general conclusion that the astronomical bands in the 10.5 to 15 μm region are dominated by emission from large neutral PAHs and small aromatic grains whereas the emission in the 5 to 9 μm region is dominated by charged PAHs.

Figure 6c shows the average spectrum of the neutral, cation, and anion forms of the PAHs considered here in the CH_{oop} region. Taking the roughly 15 cm^{-1} redshift ($\sim$0.2 μm at 11 μm) expected for emission into account, this figure shows that the previous assignment of the 11.2 μm astronomical emission band to neutral PAHs and the 11.0 μm astronomical band to PAH cations (Hudgins & Allamandola 1999; Hony et al. 2001) holds for these larger species as well.

All the PAHs in this sample contain only solo and duo hydrogens. As discussed in Sect. 3.3, the solo modes for these large, compact, symmetric PAHs fall in the wavelength range expected for the CH_{oop} bend. However, this isn't the case for the duo modes. Coupling between the duo and solo CH_{oop} modes splits the duo mode into two bands (Figure 5). The longer wavelength component of the duo bands falls in the region traditionally assigned to trio bands.

Figure 9 compares the average spectrum of the neutral PAHs considered here to the spectra of NGC 7027 and IRAS 18317-0757 from Hony et al. (2001). These two object span the entire range in observed 11.2/12.7 PAH intensity ratios as observed by Hony et al. (2001). The computed spectrum is redshifted by 15 cm^{-1} to account for the emission process. The absence of bands in the computed spectrum at 11.0, 13.5, and 14.3 μm, the position of several astronomical features in Figure 9, is to be expected. These are attributed to PAH cations, and CH_{oop} bends from quartet and quintet hydrogens respectively, species and structures which are not present in the PAHs which produce the computed spectrum of large neutral PAHs. The good agreement between the strong 11.2 μm astronomical feature and the average of the computed spectra is in complete agreement with it's assignment to large, neutral PAHs.

The previously unrecognized component of the duo modes near 13 μm overlaps the astronomical emission feature at 12.8 μm which is normally attributed to trio CH_{oop} modes. This duo band impacts the interpretation of the astronomical PAH emission spectrum in two ways. First, the number of trio hydrogens deduced with respect to solo and duo hydrogens on the emitting astronomical PAH population must be reduced. The spectra shown in Figures 9 and 6c suggest that an important fraction of the intensity of the 12.8 μm astronomical feature can arise from the CH_{oop} bending vibrations from duo H's. For NGC 7027, this may be as high as 50%. This, in turn, implies that the structures Hony et al. (2001) deduced as being most important in these objects and others with spectra between 9 - 15 μm which show clear evidence for the 12 μm duo H band should be modified to more compact and symmetric forms similar to those shown in Figure 1 here. Second, this overlap between the duo and trio bands in neutral PAHs may resolve a longstanding puzzle regarding the origin of the blue shading on the 12.8 μm astronomical feature. The lower frame in Figure 9 shows that the CH_{oop} trio CH bands for small neutral PAHs fall in a narrow band, from 13.0 to 13.5 μm while the CH_{oop} duo bands for the neutral PAHs considered here range from 12.5 to 13.2 μm. Figure 6c shows this holds for the charged forms of these PAHs as well. Overlap between this duo band with the trio feature could produce the observed, blue-shaded profile.

Keep in mind that this study involves only compact, symmetric PAHs that contain only solo and duo hydrogens and that using lower symmetry species will allow more types of

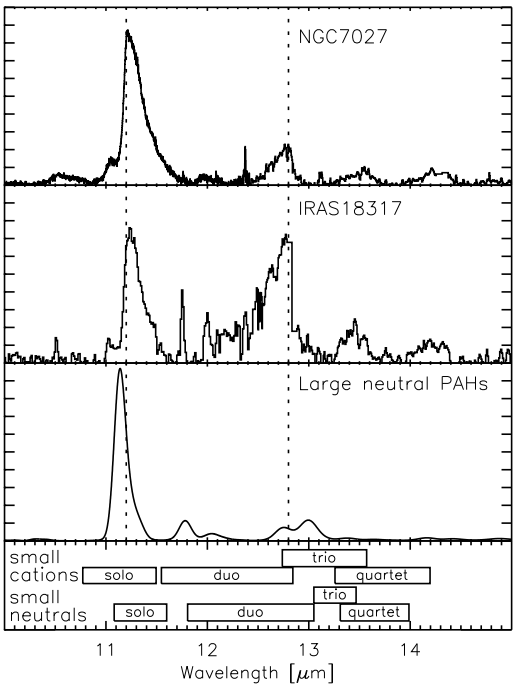

Fig. 9.— Astronomical PAH emission spectra from 10 to 15 μm compared with the average spectrum of neutral, very large PAHs. Shown are the continuum subtracted IR spectrum of the planetary nebula NGC 7027 **(top)**; the continuum subtracted IR spectrum of the HII region IRAS 18317-0757 **(second)**; the average spectrum of the neutral large PAHs considered in this paper **(third)**; and the ranges for the out-of-plane bending modes for small PAHs (C-atoms ≤ 32) (Hony et al. 2001)**(bottom)**. The data in the lower two frames have been redshifted by 15 cm^{-1} to correct for the wavelength shift between the absorption and emission process (see text).

hydrogens leading to additional couplings. These results suggest that caution is warranted when constraining the number and nature of adjacent hydrogens and implied structures using the out-of-plane bending modes alone. This issue is considered further in paper II which treats the spectra of less symmetric and less compact very large PAHs.

5. Conclusions

The mid-IR spectra of seven very large, compact, symmetric PAHs with formulae $C_{54}H_{18}$, $C_{66}H_{20}$, $C_{78}H_{22}$, $C_{96}H_{24}$, $C_{110}H_{26}$, $C_{112}H_{26}$, and $C_{130}H_{28}$ have been determined computationally using Density Functional Theory (DFT). Previous to this study, the mid-IR spectroscopic properties of PAHs was essentially limited to species containing about 50 or fewer carbon atoms. These data provide new insight into the effect of size, structure and charge on PAH IR spectra and enhances our understanding of the PAH populations that contribute to the observed astronomical spectra. The main conclusions regarding the principle astronomical emission features follow.

The 3.29 μm Feature: The strongest feature in the CH stretching region near 3.3 μm is similar for all PAH species considered in this work. The peak position of this band in these compact, very large PAHs falls within the regions expected based on the spectroscopy of smaller PAHs, but covers a narrower range. While clearly ruling out an origin in PAH cations, these spectra suggest that the astronomical $A_{3.3}$ and $B_{3.3}$ bands reflect the relative contribution of PAH neutrals and anions.

The 5 - 9 μm Features: Consistent with earlier work on smaller PAHs, the intensities of the major features between 5 and 9 μm in these larger PAHs are enhanced by an order of magnitude or more upon ionization.

The dominant bands in the CC stretching region between 6.1 and 6.4 μm show less variation in the spectra of the anions than in the spectra of the cations and they are slightly weaker relative to the bands between 7 and 9 μm. The average band in the cation and anion spectra peaks slightly redward of 6.3 μm, far to the red of the astronomical 6.2 μm band. Thus, as with small PAHs, the CC stretch in large PAHs comprised of only C and H cannot reproduce the peak position of the astronomical feature, reinforcing our previous suggestion that astronomical PAHs contain nitrogen (PANHs, Peeters et al. 2002a; Hudgins et al. 2005).

The largest PAH cations and anions considered have strong bands close to 7.7 μm, the position of the strongest astronomical emission feature. The strong feature produced by the cations and anions overlap to a large extent, but the average anion peak falls about 0.1 μm to the red of the average cation peak. These data suggest that the astronomical 7.7 μm

band is produced by overlapping bands from a mixture of small and large PAH cations and anions, with small PAHs contributing more to the 7.6 μm component and large PAHs more to the 7.8 μm component. This implies that the variation in the peak position of the 7.8 μm feature may be related to the variation in relative amounts of large PAH cations and anions since negatively charged large PAHs emit at slightly longer wavelenths than do the PAH cations.

A band near 8.5 μm grows in strength and shifts slightly to the red as PAH size increases for both anions and cations. The bands from both the large PAH anions and cations overlap, with the anions contributing more strongly at slightly longer wavelengths. Peeters et al. (2002a) found a correlation between the peak position of the astronomical 7.7 μm feature and that of the 8.6 μm band. The inability of small PAHs to reproduce this correlation suggests that the astronomical 7.8 μm component and the 8.6 μm feature originate primarily in large, cationic and anionic PAHs, with the specific peak position and profile reflecting the particular cation to anion concentration ratio in any given object.

The 10 - 15 μm Features: The prominent features that span this region correspond to CH_{oop} bending vibrations. The large PAHs in this sample contain only solo and duo hydrogens. The solo modes for these large, compact, symmetric PAHs fall in the wavelength range expected for the solo CH_{oop} bend. However, this isn't the case for the duo CH_{oop} modes. The duo and solo CH_{oop} vibrations couple in these large, compact PAHs, causing a splitting of the duo band. One component remains close to the traditional duo band position while the other shifts to about 13 μm, the region traditionally assigned to trio bands.

The excellent agreement between the strong 11.2 μm astronomical feature and the average of the computed spectra for neutral PAHs presented here lends strong support to its assignment to large, neutral astronomical PAHs. However, the previously unrecognized component of the duo modes near $\sim$12.8 μm overlaps the astronomical emission feature at 12.8 μm which is normally attributed to trio CH_{oop} modes. This overlap impacts the interpretation of the astronomical PAH emission spectrum in two ways. The number of trio hydrogens deduced with respect to solo and duo hydrogens on the emitting astronomical PAH population must be reduced, in some cases, by as much as a factor of two, implying that the PAH structures Hony et al. (2001) previously deduced should be modified to favor more compact and symmetric forms. Second, the overlap between the duo and trio bands in neutral PAHs may produce the puzzling, blue-shaded profile of the 12.8 μm feature that is commonly observed.

The spectra of comparable large, but less symmetric PAHs will be presented and discussed in a forthcoming publication.

We very gratefully acknowledge sustained support from NASA's Long Term Space Astrophysics and Astrobiology Programs, and the Spitzer Space Telescope Archival and General Observer Program.

REFERENCES

Allamandola, L. J., Tielens, A. G. G. M., & Barker, J. R. 1989, ApJS, 71, 733

Bauschlicher, C. W. 2002, ApJ, 564, 782

Bauschlicher, C. W. & Bakes, E. L. O. 2000, Chem. Phys., 262, 285

Bauschlicher, C. W. & Langhoff, S. R. 1997, Spectrochim. Acta, 53, 1225

Becke, A. D. 1993, J. Phys. Chem., 98, 5648

Brandl, B. R., Bernard-Salas, J., Spoon, H. W. W., et al. 2006, ApJ, 653, 1129

Bregman, J. & Temi, P. 2005, ApJ, 621, 831

Brenner, J. & Barker, J. R. 1992, ApJ, 388, L39

Colangeli, L., Mennella, V., & Bussoletti, E. 1992, ApJ, 385, 577

Compiègne, M., Abergel, A., Verstraete, L., et al. 2007, A&A, 471, 205

Cook, D. J. & Saykally, R. J. 1998, ApJ, 493, 793

Cox, P. & Kessler, M., eds. 1999, The Universe as Seen by ISO, ESA-SP 427

Draine, B. T. & Li, A. 2007, ApJ, 657, 810

Flickinger, G. C., Wdowiak, T. J., & Gomez, P. L. 1991, ApJ, 380, L43

Frisch, M. J., Pople, J. A., & Binkley, J. S. 1984, J. Phys. Chem., 80, 3265

Frisch, M. J., Trucks, G. W., Schlegel, H. B., et al. 2003, Gaussian 03, Revision B.05, Gaussian, Inc., Pittsburgh PA

Galliano, F., Madden, S., Tielens, A., Peeters, E., & Jones, A. 2008, ApJ, 000, 000

Helou, G., Lu, N. Y., Werner, M. W., Malhotra, S., & Silbermann, N. 2000, ApJ, 532, L21

Hony, S., Van Kerckhoven, C., Peeters, E., et al. 2001, A&A, 370, 1030

Hudgins, D. M. & Allamandola, L. J. 1999, ApJ, 516, L41

Hudgins, D. M., Bauschlicher, C. W., & Allamandola, L. J. 2001, Spectrochimica Acta, 57, 907

Hudgins, D. M., Bauschlicher, Jr., C. W., & Allamandola, L. J. 2005, ApJ, 632, 316

Joblin, C., Abergel, A., Bregman, J., et al. 2000, ISO beyond the peaks: The 2nd ISO workshop on analytical spectroscopy. Eds. A. Salama, M.F.Kessler, K. Leech & B. Schulz. ESA-SP, 456, 49

Joblin, C., Boissel, P., Leger, A., D'Hendecourt, L., & Defourneau, D. 1995, A&A, 299, 835

Langhoff, S. R. 1996, J. Phys.Chem., 100, 2819

Li, A. 2004, in Astronomical Society of the Pacific Conference Series, Vol. 309, Astrophysics of Dust, ed. A. N. Witt, G. C. Clayton, & B. T. Draine, 417

Li, A. & Draine, B. T. 2001, ApJ, 554, 778

Li, A. & Draine, B. T. 2002, ApJ, 572, 232

Malloci, G., Joblin, C., & Mulas, G. 2007, A&A, 462, 627

Mattioda, A. L., Allamandola, L. J., & Hudgins, D. M. 2005, ApJ, 629, 1183

Onaka, T. 2004, in Astronomical Society of the Pacific Conference Series, Vol. 309, Astrophysics of Dust, ed. A. N. Witt, G. C. Clayton, & B. T. Draine, 163

Pathak, A. & Rastogi, S. 2006, in COSPAR, Plenary Meeting, Vol. 36, 36th COSPAR Scientific Assembly, 432

Peeters, E., Allamandola, L. J., Hudgins, D. M., Hony, S., & Tielens, A. G. G. M. 2004, in Astronomical Society of the Pacific Conference Series, Vol. 309, Astrophysics of Dust, ed. A. N. Witt, G. C. Clayton, & B. T. Draine, 141

Peeters, E., Hony, S., Van Kerckhoven, C., et al. 2002a, A&A, 390, 1089

Peeters, E., Martín-Hernández, N. L., Damour, F., et al. 2002b, A&A, 381, 571

Puget, J. L. & Léger, A. 1989, ARA&A, 27, 161

Sellgren, K., Uchida, K. I., & Werner, M. W. 2007, ApJ, 659, 1338

Sloan, G. C., Keller, L. D., Forrest, W. J., et al. 2005, ApJ, 632, 956

Smith, J. D. T., Draine, B. T., Dale, D. A., et al. 2007, ApJ, 656, 770

Snow, T. P. & Witt, A. N. 1995, Science, 270, 1455

Stephens, P. J., Devlin, F. J., Chabalowski, C. F., & Frisch, M. J. 1994, J. Phys. Chem., 98, 11623

Uchida, K. I., Sellgren, K., Werner, M. W., & Houdashelt, M. L. 2000, ApJ, 530, 817

van Diedenhoven, B., Peeters, E., Van Kerckhoven, C., et al. 2004, ApJ, 611, 928

Vermeij, R., Peeters, E., Tielens, A. G. G. M., & van der Hulst, J. M. 2002, A&A, 382, 1042

Verstraete, L., Pech, C., Moutou, C., et al. 2001, A&A, 372, 981

Williams, R. M. & Leone, S. R. 1995, ApJ, 443, 675

This preprint was prepared with the AAS LaTeX macros v5.2.